NIOZ - RAPPORT 1988 - 10

ON THE APPLICABILITY OF CAESAR FOR THE REMOTE SENSING OF BOTTOM DEPTH AND BOTTOM COMPOSITION OF SHALLOW WATERS

G. Marees, D. Spitzer

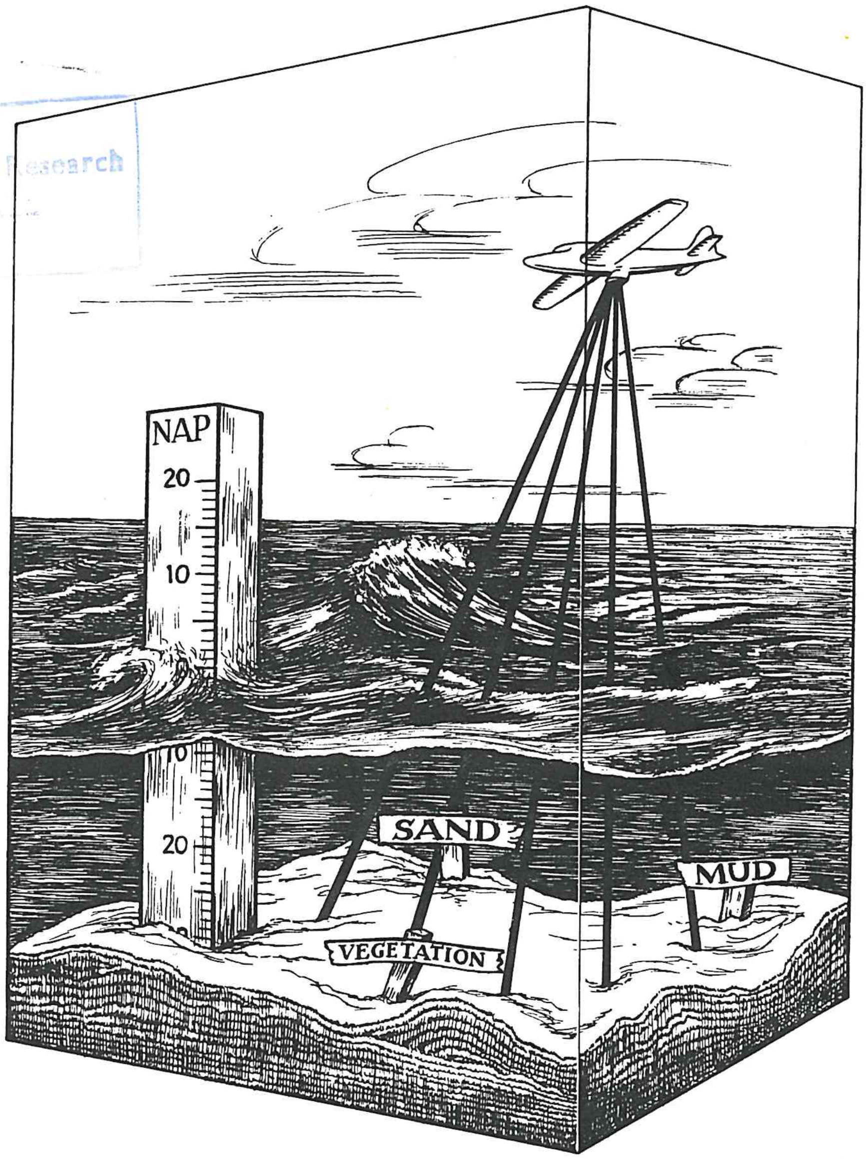

Nederlands Instituut voor Onderzoek der Zee

This is published as NIOZ - report 1988 - 10
This series was formely called:
Interne Verslagen
Nederlands Instituut voor Onderzoek der Zee
Texel

ON THE APPLICABILITY OF CAESAR FOR THE REMOTE SENSING OF BOTTOM DEPTH AND BOTTOM COMPOSITION OF SHALLOW WATERS

a model study

G. Marees (NIOZ), D. Spitzer (RWS)

This study was financially supported by the Netherlands Remote Sensing Board (B.C.R.S.)

NETHERLANDS INSTITUTE FOR SEA RESEARCH

NIOZ - RAPPORT 1988 - 10

ABSTRACT

Characteristic spectral signatures of various seawater and seabottom composition types are chosen as input parameters of a two-flow radiative transfer model. From this model waterleaving irradiance spectra are calculated for several types of seawater, bottom composition and varying bottom depths. The resulting signals for the spectral bands of the aircraft remote sensing scanner CAESAR are computed in order to deduce appropriate algorithms for remote determination of bottom depth and bottom composition.

The deduced CAESAR bottom algorithms are found to be more accurate than similar algorithms earlier found for Landsat Thematic Mapper. In case of clear water in combination with a sandy bottom composition, CAESAR can detect the bottom features down to depths of 24-31 m.

1. INTRODUCTION

Since conventional shipboard bathymetric surveying of shallow waters is time and manpower consuming, interest has been raised in recent years in the application of remote sensing techniques for mapping of bottom features. In this report the applicability of the multispectral aircraft scanner CEASAR for remote determination of such bottom features is treated.

In shallow waters, the waterleaving irradiance spectra are not only determined by absorption and scattering of downwelling solar irradiance in the watercolumn. Also the reflection of irradiance at the seabottom is of substantial influence on these spectra. Due to the bottom reflection contribution to the waterleaving irradiance spectra, the algorithms developed for the remote determination of concentrations of dissolved and suspended materials in deep waters are not suited for shallow waters. Inversely, when a significant fraction of the irradiance is reflected at the bottom, the corresponding excess waterleaving irradiance provides information on the bottom features.

Previously some studies about the remote determination of bottom depth and/or bottom composition have been performed. Gordon and McCluney (1975) investigated the penetration depth of solar irradiance in natural waters. Lyzenga (1978,1981 1985) described both passive as well as active remote sensing techniques for mapping bottom depth and bottom features. Parades and Spero (1983) discussed some algorithms for passive remote sensing of bottom depth. From a theoretical two-flow radiative transfer model in combination with characteristic spectral signatures of several seawater and seabottom types, Spitzer and Dirks (1987) developed algorithms for mapping bottom depth and bottom composition which are suited for Landsat MSS and TM, Spot HRV and the NOAA-AVHRR scanners. An atmospheric radiative transfer model to be used in combination with the algorithms for Landsat TM was presented by van Hengel and Spitzer (1987).

In this report a model similar to that of Spitzer and Dirks (1987) is used to compute algorithms appropriate for the spectral bands of the airborne remote sensing instrument CAESAR (CCD Airborne Experimental Scanner for Application in Remote sensing) (Pouwels, 1987). The main advantage of CAESAR over the above mentioned satellite scanners is that more spectral bands are available in the visible part of the spectrum (6 bands, bandwidth ≈ 20 nm). A second advantage is that the spatial resolution of CAESAR (1.5 x 3.7 m) is much higher than these of Landsat and Spot (20 - 30 m). The high spatial resolution makes CAESAR very well suited for mapping of waters with highly variable bottom composition and/or depth. For instance, CAESAR could be used for a periodic check of bottom depths in coastal channels. Orbital and meteorological conditions limit the number of suitable TM and SPOT imagery per year. CAESAR might be available at call when the environmental conditions are suitable.

2. THEORETICAL BACKGROUND

The bottom algorithms which are presented in this report are deduced from results of a radiative transfer model which is treated in detail by Dirks and Spitzer (1987). The main result of interest of this theory for the present study is that the variation of the irradiance reflectance R (by definition the ratio of the upwelling (index u) and downwelling (index d) irradiance) changes with depth z according to the Ricatti equation:

$$dR(z)/dz = -b_d(z) + [c_u(z) + c_d(z)]R(z) - b_u(z)R^2(z) \qquad \ldots(1)$$

with: $a_u=D_ua$ $\quad$ $a_d=D_da$

$b_u=D_ub$ $\quad$ $b_d=D_db$

$c_u=a_u+b_u$ $\quad$ $c_d=a_d+b_d$

Since shallow waters are generally vertically well mixed, the absorption coefficient a(λ) and backscattering coefficient b(λ) have been treated in this report as depth independent. D_u and D_d are the distribution functions for upwelling and downwelling irradiance, respectively. According to Preisendorfer (1976) D_u and D_d can be treated as both depth and wavelength independent. Because of the poor water penetrating ability of red light, the band 6 of CAESAR (675 - 695 nm) was not used for the algorithm development. Thus the fluorescence effects (Spitzer and Dirks, 1985,1986) are further not treated.

With the reflectance boundary condition $R(h)=R_b$, where h is the bottom depth and R_b the bottom reflectance coefficient, the solution of eq.1 can be expressed as:

$$R_o = R_q + \frac{(R_q - R_\alpha)\dfrac{(R_b - R_q)}{(R_b - R_\alpha)}\exp(-\chi h)}{1 - \dfrac{(R_b - R_q)}{(R_b - R_\alpha)}\exp(-\chi h)} \qquad \ldots(2)$$

with R_o the irradiance reflectance just beneath the air-water interface, $R_{q,\alpha} = (c \mp \chi)/2b_u$, $\chi = \sqrt{c^2 - 4b_u b_d}$ and $c = c_u + c_d$. For most natural waters b/a <<1, yielding in good approximation:

$$R_o = R_\infty + (R_b - R_\infty)e^{-\chi h} \qquad \ldots(3)$$

with the deep water reflectance $R_\infty = R_q = b_d/\chi$ and $\chi \approx a_u + a_d$. For the calculations in this report we used eq.3. Lyzenga (1978,1981,1985) and Parades and Spero (1983) assumed

$$R_o = R_\infty + R_b e^{-\chi h} \qquad \ldots(4)$$

i.e. $R_\infty \ll R_b$. This is especially in the case of a mud or a vegetation type bottom a crude approximation (see fig.3).

The upwelling radiance signal, $L_u(\lambda)$, integrated over the CAESAR spectral band i can be expressed as:

$$C_i = \int_{B_i} L_u(\lambda) S(\lambda) d\lambda = \int_{B_i} \frac{1-\rho}{n^2} \frac{R_o(\lambda) E_d(\lambda) S(\lambda)}{Q} d\lambda \qquad \ldots(5)$$

where ρ is the fresnel reflectivity of the water surface, n the reflective index of seawater, E_d the downwelling solar irradiance at sea level and Q the solid angle factor. B_i is the bandwidth of spectral band i and $S(\lambda)$ is the spectral sensitivity of the scanner (Pouwels,1987). For our model calculations we assumed $S(\lambda)$=constant over the bandwidths. It should be mentioned that atmospheric influences and sunglitter effects on C_i are not treated in this report.

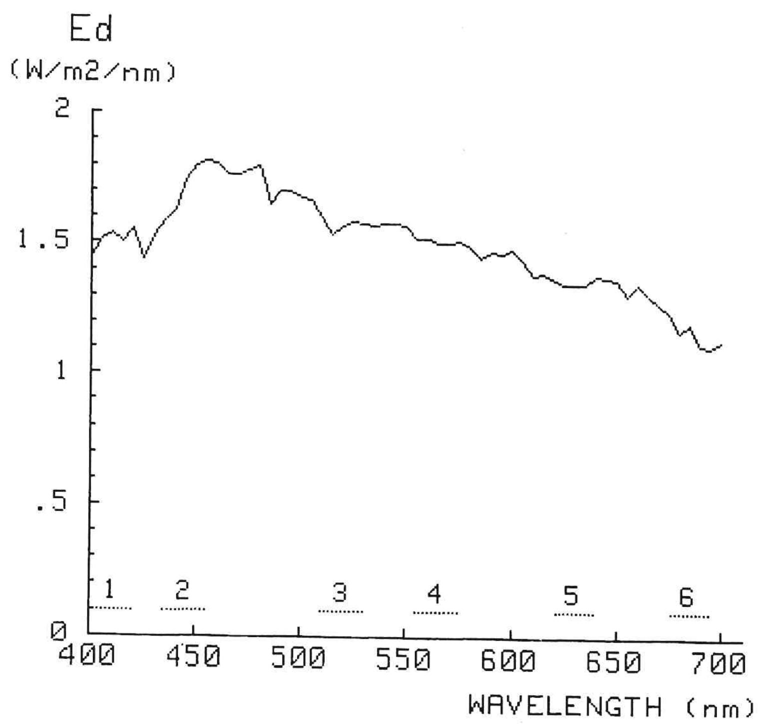

Fig.1 Characteristic downwelling irradiance spectrum at sea level and for clear sky conditions. Location and number of the CAESAR spectral bands are indicated.

3. INPUT PARAMETERS

The solid angle factor Q in eq.5 is assumed to be 5, the factor $(1-\rho)/n^2$, representing the irradiance transmission through the water-air interface, is chosen to be 0.54 (Sathyendranath and Morel,1983). A characteristic downwelling irradiance spectrum $E_d(\lambda)$ at sea level ($z=0$) and for clear sky conditions, is tabulated by Tyler and Smith (1970). The corresponding graph is shown in fig.1. Location and number of the CAESAR spectral bands are also indicated in this figure.

For the absorption and the backscattering coefficients we used the standard classification:

$$a=a_w+a_c+a_p+a_y$$
$$b=b_w+b_c+b_p \qquad (b_y=0) \qquad \ldots(6)$$

where the index w refers to pure seawater, c to particulate chlorophyllous material, p to particulate non-chlorophyllous material and y to the yellow substance component (the coloured component of dissolved organic matter). Specific absorption and backscattering coefficients are given by:

$$a_c=Ca_c^* \quad a_p=Pa_p^* \quad b_c=C^{0.63}b_c^* \quad b_p=Pb_p^*$$

with C the total pigment concentration in mg/m^3 determined by standard methods and P the concentration of non-chlorophyllous particles in terms of the total scattering coefficient in m^{-1} (Prieur and Sathyendranath, 1981). The yellow substance concentration Y is expressed by means of its absorption coefficient at 380 nm, $Y=a_y(380)$, in m^{-1}.

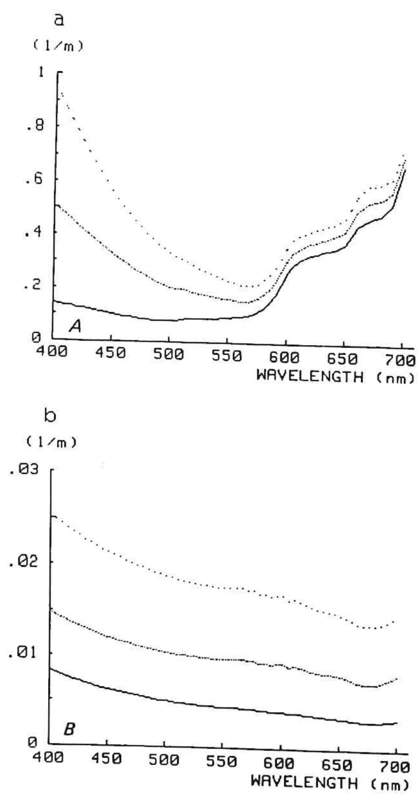

Fig.2 The absorption coefficient (fig.2a) and backscattering coefficient (fig.2b) as function of wavelength. The lower full curves represent the clear water type (P=0.2 m^{-1}, Y=0.1 m^{-1} and C=0.5 mg/m^3). The curves in the middle represent the medium turbid water type (P=0.5 m^{-1}, Y=0.5 m^{-1} and C=3 mg/m^3). The upper dotted curves represent turbid coastal waters (P=1 m^{-1}, Y=1 m^{-1} and C=5 mg/m^3).

For our model calculations we used the following data sets:

$a_w(\lambda)$ and $b_w(\lambda)$ as tabulated by Smith and Baker (1981).

$a_c(\lambda)=(0.058+0.018C)a_c^{*'}(\lambda)$ with C the pigment concentration in mg/m^3 and $a_c^{*'}(\lambda)$ as tabulated by Prieur and Sathyendranath (1981).

$b_c(\lambda)=(0.005\times0.12C^{0.63})a_c^{*}(550)/a_c^{*}(\lambda)$ (Prieur, 1981).

$a_p(\lambda)=0.042\ P\ a_p^{*'}(\lambda)$, $a_p^{*'}(\lambda)$ as tabulated by Prieur and Sathyendranath (1981).

$b_p(\lambda)=0.015\ P\ (550/\lambda)$ (Prieur, 1981).

$a_y(\lambda)=a_y(380)\ \exp(-0.014(\lambda-380))$ (Bricaud et al., 1981), λ in nm.

$D_u=2.5$, $D_d=\dfrac{0.6}{\cos j}+\dfrac{0.4}{0.859}=1.2$ for the sun zenith angle (in the water) $j=35°$ (Prieur and Sathyendranath, 1981).

In this report calculations will be performed for 3 different characteristic seawater types;

1: Clear water with P=0.2 m^{-1}, Y=0.1 m^{-1} and C=0.5 mg/m^3,

2: Medium turbid water with P=0.5 m^{-1}, Y=0.5 m^{-1} and C=3 mg/m^3 and

3: Turbid coastal waters with P=1 m^{-1}, Y=1 m^{-1} and C=5 mg/m^3,

and for 3 different seabottom types;

1: sand type bottom,

2: mud type bottom and

3: vegetation type bottom.

Calculated absorption and backscattering coefficients are plotted for the 3 different seawater types as function of wavelength in figs.2a and 2b, respectively. The lower curves in

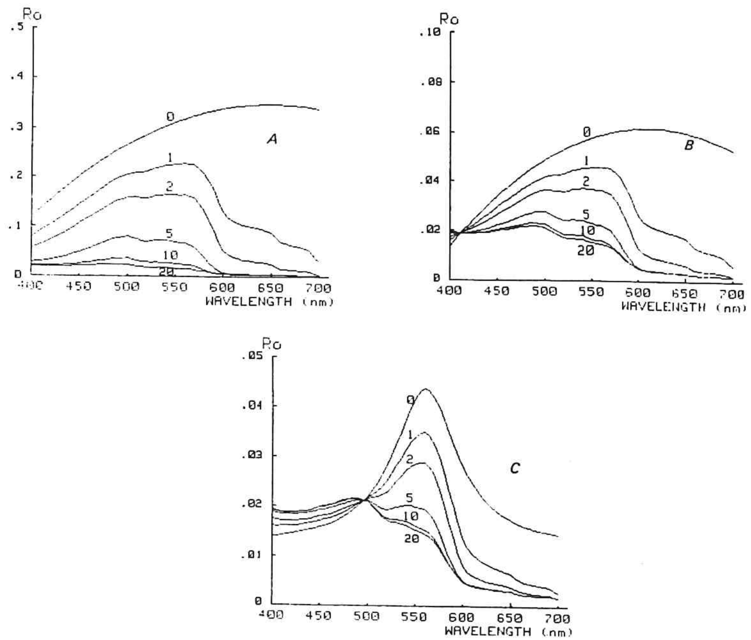

Fig.3 Irradiance reflectance spectra for the clear water type. The bottom depth in meters is indicated near each curve. The curve at zero depth represents the bottom reflection coefficient. Fig.3a shows the results found for the sand type bottom, fig.3b shows the results for the mud type bottom and fig.3c the results for the vegetation type bottom.

fig.2 represent the clear water situation, the curves in the middle represent the medium turbid water situation, and the upper dotted curves represent turbid coastal waters.

Characteristic bottom reflectance spectra of sand, mud and vegetation, $R_s(\lambda)$, $R_m(\lambda)$ and $R_v(\lambda)$, were determined in the laboratory using an optical multispectral analyzer (Spitzer and Dirks, 1987).

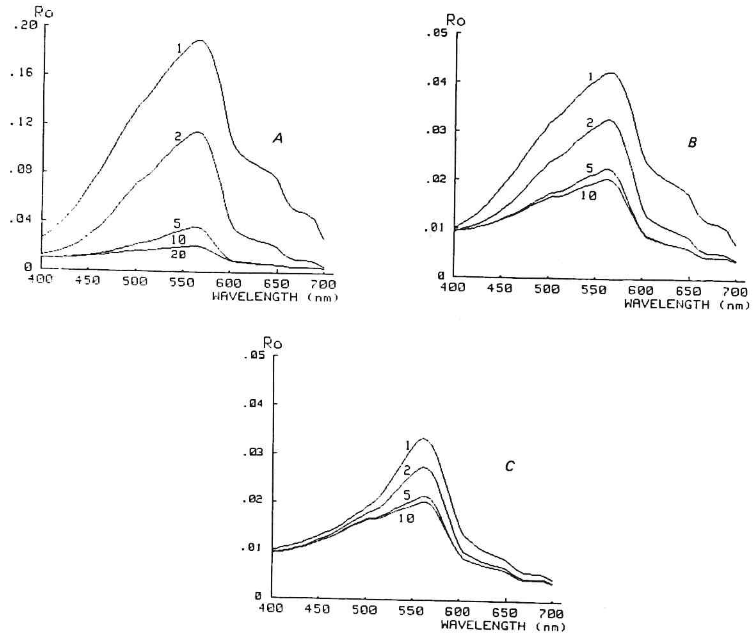

Fig.4 Irradiance reflectance spectra for the medium turbid water type. The bottom depth in meters is indicated near each curve. Fig.4a shows the results found for the sand type bottom, fig.4b shows the results for the mud type bottom and fig.4c the results for the vegetation type bottom.

4. RESULTS

From eq.3 in combination with the input parameters defined in the previous section, the irradiance reflectance spectra are computed for various water types, bottom compositions and bottom depths. The clear water reflectance spectra are shown in fig.3. For the sand type bottom in fig.3a, for the mud type bottom in fig.3b and for the vegetation type bottom in fig.3c. The bottom depth in meters is indicated near each curve. The spectra for the medium turbid water situation are shown in a similar way in fig.4 and these for the turbid water situation in fig.5.

Since the reflectance spectra for zero bottom depth depend only on the bottom composition and not on the water type (at h=0 $R_o=R_b$), the zero depth spectra are only plotted in fig.3. The lowest curve in each of the subgraphs of figs.3, 4 and 5 represents the deep water reflectance (for $h=\infty$: $R_o=R_\infty$). Generally, the calculated reflectance increases with decreasing bottom depth, most pronounced at the center wavelengths. Notice that in fig.3c the vegetation bottom reflectance (curve for zero depth) in the blue part of the spectrum is smaller than the deep water reflectance. In this special case the reflectance decreases with decreasing bottom depth. Large irradiance absorption in the blue part of the spectrum due to the bottom vegetation causes this phenomenon.

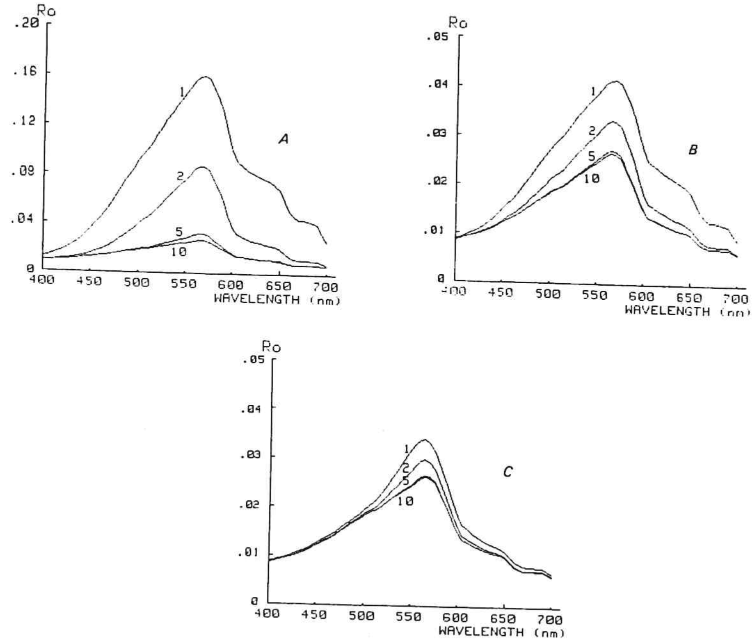

Fig.5 Irradiance reflectance spectra for the turbid water type. The bottom depth in meters is indicated near each curve. Fig.5a shows the results found for the sand type bottom, fig.5b shows the results for the mud type bottom and fig.5c the results for the vegetation type bottom.

4.1 BOTTOM DEPTH ALGORITHMS

It follows immediately from eq.3 and 5 that if the water optical properties and the bottom reflectance coefficient are uniform for a sea area, a good correlation will exist between the bottom depth and the collected radiance in a single spectral band.

For accurate remote determination of bottom depths, bottom depth algorithms should be insensitive to variations of bottom composition and water quality and preferably linear with respect to bottom depth. The irradiance reflectance R_o found just beneath the sea surface is exponentially dependent on the bottom depth (eq.3). Thus a logarithmic transformation of C_i will yield expressions linear with respect to depth. Lyzenga (1978,1981,1985) showed that transformations of the type $ln(C_i-C_{i\infty})$ were the most advantageous (where $C_{i\infty}$ is the integrated upwelling radiance signal of CAESAR band i over deep waters (eq.5)). The bottom algorithms treated in this report are all linear combinations of expressions of the type: $ln(C_i-C_{i\infty})$. The change of $ln(C_i-C_{i\infty})$ with bottom depth for clear water in combination with a sandy bottom type is shown as an example in fig.6. The limiting depth for these "subalgorithms" is reached when the condition $(C_i-C_{i\infty})/C_{i\infty}$ becomes smaller than the corresponding noise equivalent reflectance of the specific spectral band (Pouwels,1987). Graphs similar to these of fig.6 have been made for various water qualities and bottom compositions.

In this report we will use the same classification for the bottom depth algorithms as Spitzer and Dirks (1987), who

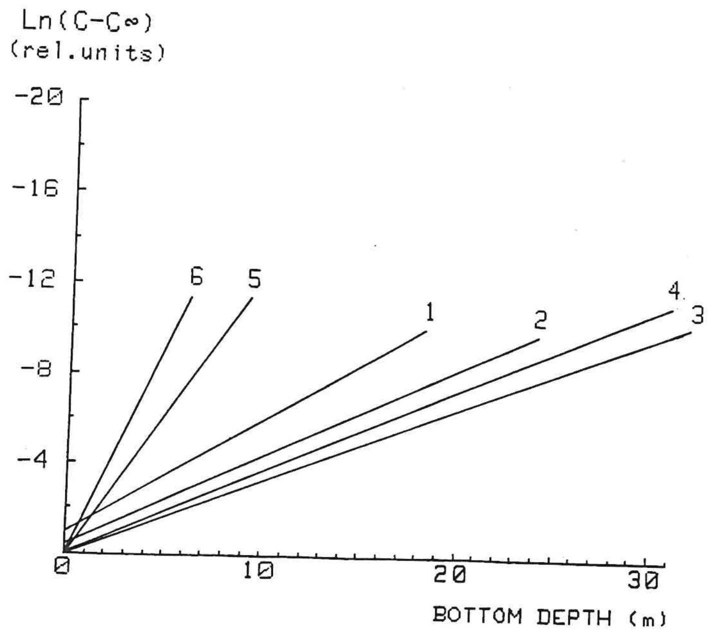

Fig.6 The change of $ln(C_i-C_{i\infty})$ as function of bottom depth for the 6 CAESAR spectral bands (i=1 to 6). This graph shows the result for the clear water type in combination with the sand type bottom.

introduced a type 1 and a type 2 algorithm. Bottom depth algorithm type 1 reads as:

$$Az_1=ln((C_i-C_{i\infty})/(C_j-C_{j\infty})) \quad ...(7a)$$

combining eq.3,5 and 7a yields:

$$Az_1=h(\chi_j-\chi_i) + (1-\varepsilon)\,ln((R_{bj}-R_{j\infty})/(R_{bi}-R_{i\infty})) \quad ...(7b)$$

the small term ε accounts for the fact that the influence of $E_d(\lambda)$ on C_i (see eq.5) depends on the specific spectral band. In eqs.7, $\chi_i, \chi_j, R_{bi}, R_{bj}, R_{i\infty}$ and $R_{j\infty}$ represent mean values over the CAESAR bands.

The depth dependence of Az_1 is fully determined by the water quality parameters χ_i and χ_j, the "intersection" depends on both water quality and bottom composition (R_∞ and R_b , respectively).

From a systematic investigation of all spectral band combinations the algorithm least sensitive for variable water quality and bottom composition was found to be

$$Az_1=ln((C_4-C_{4\infty})/(C_5-C_{5\infty})) \quad ...(8)$$

In fig.7a the result is shown for the clear water type and the 3 different bottom compositions. Fig.7b shows the results found for a sandy bottom composition and the 3 different water types. Not all the lines are shown in a single graph for clarity.

The accuracy of the Az_1 algorithm is very good, the maximal depth uncertainty is ± 0.7 m. The penetration depth is rather small (≤ 9 m, depending on water type and bottom composition) and it is indicated for each line by means of the vertical dotted

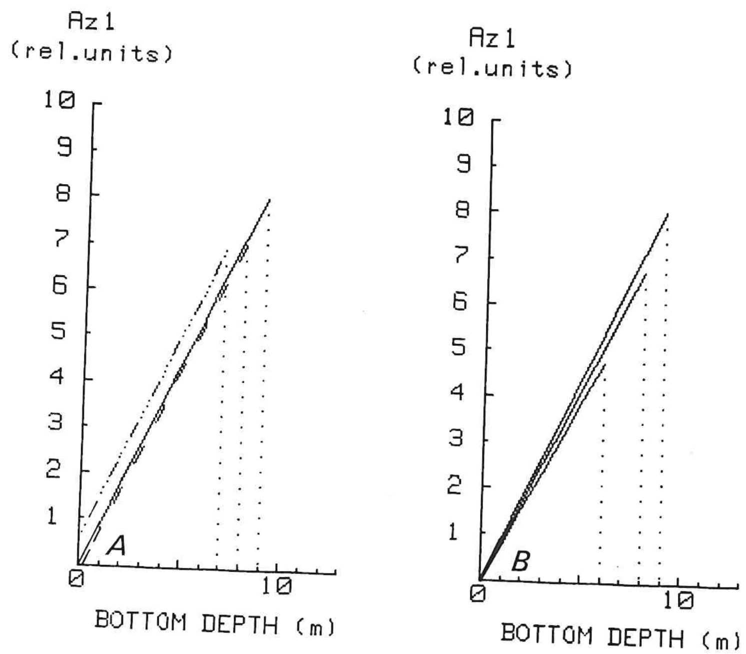

Fig.7 Algorithm $Az_1 = ln(C_4 - C_{4\infty}) - ln(C_5 - C_{5\infty})$ as function of bottom depth. Fig.7a shows the result for the clear water type. The full line represents the sand type bottom, the dashed line the mud type bottom and the dotted-dashed line the vegetation type bottom. Fig.7b shows the result for the 3 water types in combination with the sand type bottom. Obviously, the long line represents the clear water type, etc. The limiting values of detectable depths are indicated for each line.

lines. This small penetration depth is caused by the large attenuation of orange/red light (CEASAR band 5) in water (see fig.2). For all type 1 algorithms, however, the use of band 5 is essential to get an accurate depth algorithm.

A much larger penetration depth is found when combinations of the CAESAR bands 1 to 4 are used in the so-called type 2 algorithm. The general shape of the type 2 algorithms can be expressed as

$$Az_2 = \sum_i k_i\, ln(C_i - C_{i\infty}) \propto \sum_i k_i\, ln(R_{bi} - R_{i\infty}) - h \sum_i k_i \chi_i \qquad \ldots(9)$$

where k_i are constants (notice that when $k_1 = -k_2 = 1$ $Az_1 = Az_2$). The change of the expression $ln(C_i - C_{i\infty})$ with bottom depth is known for the various water types and bottom compositions (see fig.6). Thus also the change of Az_2 (which is a linear combination of such expressions) with depth can be calculated. The best choice for k_i is such that $Az_2(h)$ is independent of both water quality and bottom composition.

The optimum result we have found for a 3 band algorithm (bands 2, 3 and 4) reads as:

$$Az_2 = 5.15\left[ln(C_3 - C_{3\infty}) - ln(C_4 - C_{4\infty})\right] - ln(C_2 - C_{2\infty}) \qquad \ldots(10)$$

Fig.8 shows the result for the various situations. The maximal inaccuracy of Az_2 for bottom depth determination is ± 2 m. This inaccuracy is larger than the corresponding one for the Az_1 algorithm. The penetration depth of Az_2, however, is also much larger than these of Az_1 (up to 24 m, depending on water type and

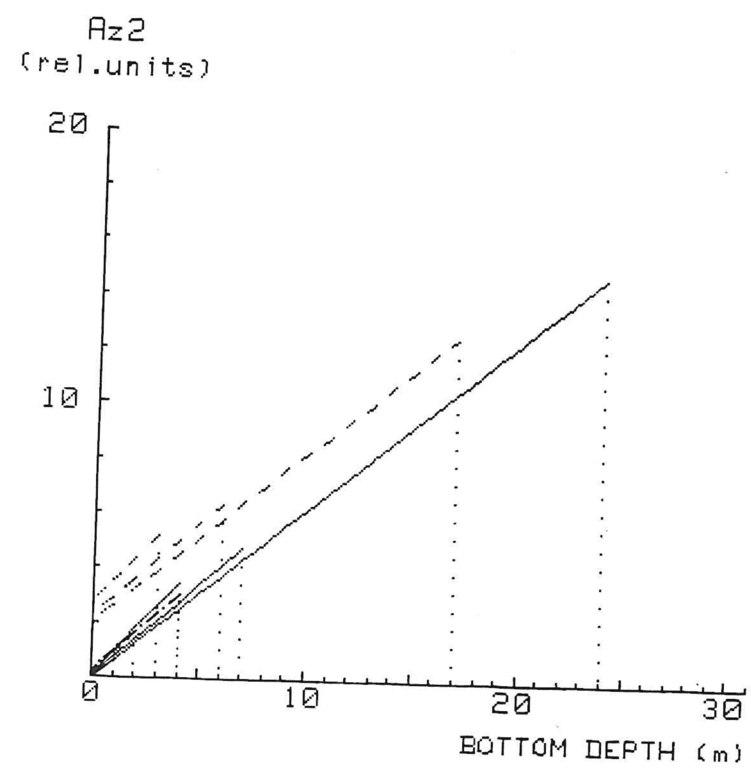

Fig.8 Algorithm $Az_2=5.15\left(ln(C_3-C_{3\infty})-ln(C_4-C_{4\infty})\right)-ln(C_2-C_{2\infty})$ as function of bottom depth. The 3 full lines represent results found for the sand type bottom for clear, medium turbid and turbid waters. The 3 dashed lines represent the mud type bottom at the 3 different water types. The 2 dotted-dashed lines represent the results for the vegetation type bottom for medium turbid and turbid waters. Again the longer lines represent the clear water type, etc. The limiting values of detectable depths are indicated for each line.

bottom composition). This makes Az_2 more suitable than Az_1 for the mapping of deep waters. It should be mentioned that incorporating also the signal of CAESAR band 1 in Az_2 does not result in a more accurate algorithm, only the penetration depth becomes smaller!

A disadvantage of the use of Az_2 in its present form is that it is less suited for mapping bottom depths over vegetation type bottoms. The large irradiance absorption by the bottom vegetation causes that for clear waters $(C_2-C_{2\infty})<0$ and thus that $ln(C_2-C_{2\infty})$ is inconsistent.

Omitting the signal of band 2, and just using the signals of CAESAR bands 3 and 4 in a type 2 bottom depth algorithm has the advantage that also for the combination clear water and a vegetation type bottom a suitable algorithm can be deduced. A second advantage is that also the maximal penetration depth is larger than for the 3 band Az_2 algorithm. The accuracy, however, is somewhat smaller.

The best result for a 2 band bottom depth algorithm is found to be:

$$Az_{22}=0.6ln(C_3-C_{3\infty}) - ln(C_4-C_{4\infty}) \qquad ...(11)$$

The result of Az_{22} for the various water types and bottom compositions is depicted in fig.9. Fig.9a shows the results for the mud bottom and for the sand bottom. Fig.9b shows results for the vegetation bottom and again for the sand bottom (not all the lines have been plotted in a single graph for clarity).. The maximal depth inaccuracy of algorithm Az_{22} is ± 2.7 m. The penetration depth (for a sand bottom and clear water) is 31 m.

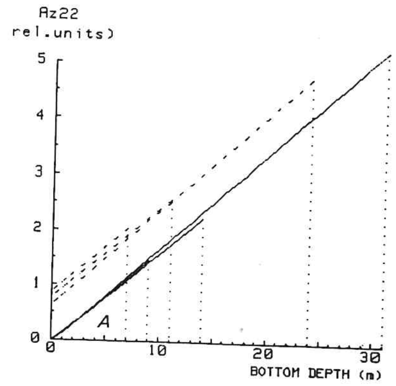

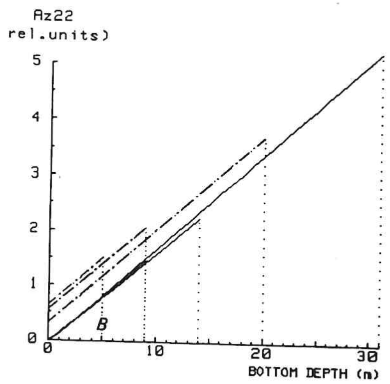

Fig.9 Algorithm $Az_{22}=0.6 ln(C_3-C_{3\infty})-ln(C_4-C_{4\infty})$ as function of bottom depth. Fig.9a shows results for the sand type bottom (full lines) and the mud type bottom (dashed lines) for the 3 different water types. Fig.9b shows the results for the vegetation type botton (dotted-dashed lines) and again the sand type bottom (full lines). Again the longer lines represent the clear water type, etc. The limiting values of detectable depths are indicated for each case.

4.2 BOTTOM COMPOSITION ALGORITHMS

Not only the bottom depth but also the bottom composition can be determined remotely by using suitable algorithms. Bottom composition algorithms should be insensitive to changes of both bottom depth and water type. A procedure to deduce suitable bottom composition algorithms is presented in this section.

From eq.3, combined with eq.5, it follows that the "subalgorithm":

$$Ab_s=\chi_j ln(C_i-C_{i\infty}) - \chi_i ln(C_j-C_{j\infty}) \qquad ...(12)$$

can be transformed as: $Ab_s \propto ln(R_{bi}-R_{i\infty}) - \frac{\chi_i}{\chi_j} ln(R_{bj}-R_{j\infty})$

Thus Ab_s is independent on bottom depth for a specific water quality (χ_i and χ_j are avaraged values over the spectral bands). The next step is to find a second depth independent subalgorithm at the same water quality but for another spectral band combination. It is obvious that also each linear combination of these two subalgorithms is depth independent for the specific water quality. We found, however, that some specific linear combinations are also (almost) depth independent for other water qualities.

The most suitable bottom composition algorithm appeared to be

$$Ab_1= 2.93 ln(C_2-C_{2\infty}) - 10.4 ln(C_3-C_{3\infty}) + 6.0 ln(C_4-C_{4\infty}) \qquad ...(13)$$

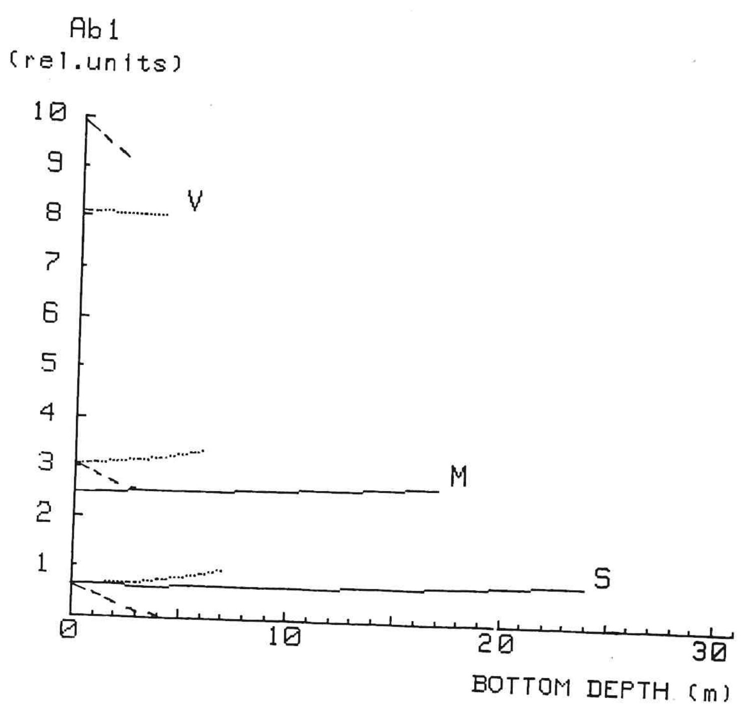

Fig.10 Algorithm $Ab_1=2.93ln(C_2-C_{2\infty})-10.4ln(C_3-C_{3\infty})+6.0ln(C_4-C_{4\infty})$ as function of bottom depth. The symbols S, M and V indicate the different bottom types. S=sand bottom, M=mud bottom and V=vegetation bottom. Full lines represent the clear water type, dotted lines the medium turbid water type and the dashed lines the turbid water type.

Fig.10 shows the results for various bottom composition types and water types. The symbols indicate the different bottom types: S=sand bottom, M=mud bottom and V=vegetation bottom. The lines representing the clear water situation (the full drawn lines in fig.10) are depth independent. These for the medium turbid water (dotted lines) and the turbid water (dashed lines) are almost depth independent. It should be mentioned that the use of the signals of CAESAR band 1 and/or 5 in Ab_1 deteriorates the accuracy of the algorithm.

The Ab_1 algorithm is not well suited for a direct detection of vegetation bottoms in combination with a clear water type because of the use of band 2 (see previous subsection). No suitable bottom composition algorithm without band 2 could be found, however. But when the bottom depth is known to be less than 20 m (from algorithm Az_{22}) and it is found that $C_2 < C_{2\infty}$, a vegetation type bottom will be present.

For pixels with a uniform bottom composition the value of Ab_1 unambiguously predicts the correct bottom type. When two different bottom types cover a single pixel it will be shown that Ab_1 can also predict the fraction of each of the two components: The total bottom reflectance can be expressed as

$$R_b=SR_s + MR_m + VR_v \qquad ...(14)$$

where S, M and R are the bottom fractions covered by sand, mud and vegetation, respectively. Obviously S+M+V=1. From eq.5 together with eqs.3 and 14 Ab_1 can be computed as a function of pixel coverage.

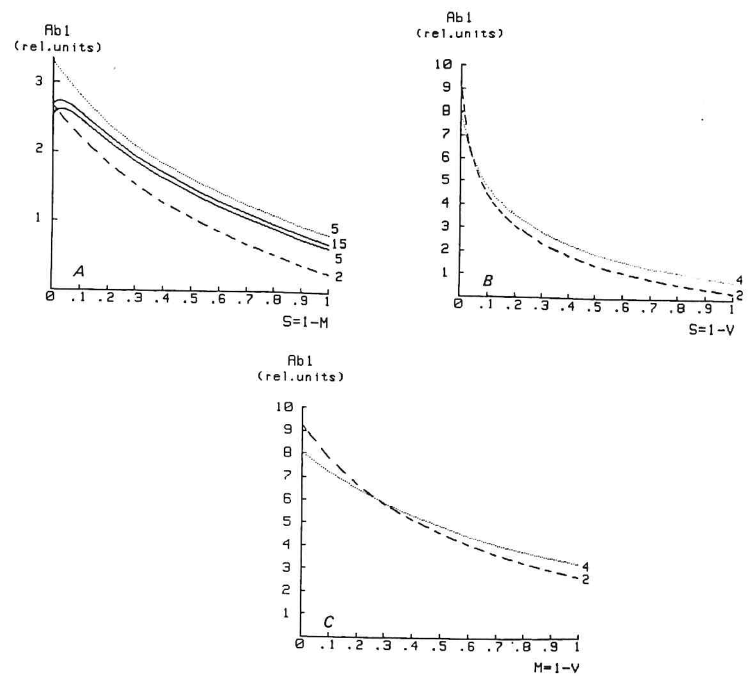

Fig.11 Algorithm $Ab_1=2.93\ln(C_2-C_{2\infty})-10.4\ln(C_3-C_{3\infty})+6.0\ln(C_4-C_{4\infty})$ as function of pixel coverage. Full curves represent the clear water type, dotted curves the medium turbid water type and dashed curves the turbid water type. The bottom depth in meters is indicated near each curve. Fig.11a shows Ab_1 for the sand/mud bottom type (S=1-M,V=0), fig.11b shows Ab_1 for the sand/vegetation bottom type (S=1-V,M=0) and fig.11c shows Ab_1 for the mud/vegetation bottom type (M=1-V,S=0).

Some examples are shown in fig.11. Fig.11a shows Ab_1 as a function of the sand fraction S for a sand/mud bottom type (S=1-M,V=0). The drawn curves represent clear water situations, the upper dotted curve represents the medium turbid water situation and the lower dashed curve the turbid water situation. Similar curves are displayed in fig.11b for a sand/vegetation bottom and in fig.11c for a mud/vegetation bottom. The bottom depth in meters is indicated near each curve. It follows from fig.11 that for all 3 situations the coverage can be well estimated, irrespective of bottom depth and water quality.

The different algorithms discussed in this section are compiled in table 1, using the notation: $X_i=\ln(C_i-C_{i\infty})$.

TYPE		ALGORITHM	MAX.DEPTH (m)	Δh (m)
bottom depth	Az_1	$X_4 - X_5$	9	0.7
	Az_2	$-X_2 + 5.15X_3 - 5.15X_4$	24	2.0
	Az_{22}	$0.6X_3 - X_4$	31	2.7
bottom comp.	Ab_1	$2.93X_2 - 10.4X_3 + 6.0X_4$	24	/

TABLE 1. The deduced bottom depth and bottom composition algorithms together with their maximal penetration depth. For the bottom depth algoritms also the maximal depth inaccuracy Δh is indicated. Notation: $X_i=\ln(C_i-C_{i\infty})$.

5. DISCUSSION AND CONCLUSION

In this report we have not treated corrections necessary to eliminate the influence of the atmosphere and of sunglitter on the received signals. Under the assumption of a homogeneous atmosphere within the sensed area, the expression $ln(C_i-C_{i\infty})$ has advantages for the removal of atmospheric effects. Contributions to the signal due to the atmospheric backscattering (path radiance) will cancel out, while the transmittance of the atmosphere will yield a constant additive term in the algorithms.

The input parameters of the model (a,b,E_d,R_b) are not universal. Therefore it is essential to tune all model algorithms with in-situ information on bottom depth and/or bottom composition before application in practical situations. It would be interesting to compare input parameters especially derived for the Dutch coastal areas with these used in the model.

So far we tacidly assumed that the values of $C_{i\infty}$, determined over deep waters, are applicable in the shallow water algorithms; i.e. it is assumed that the water quality remains constant over the whole sensed region. Although it is known that the water quality remains often more or less constant over large areas because of horizontal mixing processes, there will always be a variation of water quality towards the coast. Since the change of $C_{i\infty}$ as function of water quality is much smaller than the term $C_i-C_{i\infty}$, this change can be neglected for practical purposes.

Summarizing, we can conclude that besides the better ground resolution of CAESAR, the accuracy of the CAESAR bottom algorithms is much better than the accuracy of the similar algorithms derived by Spitzer and Dirks (1987) for Landsat TM, MSS, and Spot-HRV. This is especially the case for the CAESAR type 2 algorithms. The accuracy of these algorithms is about a factor of 2 better than the similar algorithms found for Landsat TM. Contrary to the findings of Spitzer and Dirks (1987) for the satellite scanners, we have found from the model that the CAESAR scanner can unambiguously discriminate between the three different bottom types without the use of a priori knowledge on water quality and/or bottom depth.

The penetration depth found for the CAESAR algorithms is much larger than these of the satellite scanners. The CAESAR Az_{22} algorithm is applicable down to depths of 31 m. The maximal penetration depth of the Thematic Mapper algorithms was calculated by Spitzer and Dirks (1987) to be 20 m (they used the TM bands 1 and 2 : $Az_2^{tm} = ln(L_1 - L_{1\infty}) + 0.5 ln(L_2 - L_{2\infty}) + 20$).

The advantages of CAESAR over the satellite scanners are caused by the fact that CAESAR has more spectral bands with smaller bandwidth and a smaller noise equivalent reflectance than the satellite scanners (Pouwels, 1987).

In order to test the applicability of the bottom algorithms in a practical situation, preperations for a CAESAR experiment are in progress.

ACKNOWLEDGEMENTS

We would like to thank the Netherlands Remote Sensing Board (BCRS) for financial support. We acknowledge the discussions with Mr. M.R. Wernand and Drs. R.W.J. Dirks on this subject.

REFERENCES

Bricaud,A.,Morel,A., and Prieur,L, 1981, Absorption by dissolved organic matter of the sea (yellow substance) in the UV and the visible domains. Limnol. Oceanogr.,26,43.

Dirks,R.W.J., and Spitzer,D.,1987, On the radiative transfer in the sea including fluorescence and stratification effects. Limnol. Oceanogr.,32,942.

Gordon,H.R.,and McCluney,W.R.,1975, Estimation of the depth of sunlight penetration in the sea for remote sensing. Appl.Opt.,14,413.

Hengel,W.van, and Spitzer,D.,1987, Determination of the topography and the composition of the bottom in coastal seas, using Thematic Mapper imagery. Rapport no: GWAO-87.007.

Lyzenga,D.R.,1978, Passive remote sensing techniques for mapping water depth and bottom features. Appl. Opt.,17,379.

Lyzenga,D.R.,1981, Remote sensing of bottom reflectance and water attenuation parameters in shallow water using aircraft and Landsat data. Int. J. Rem. Sen.,2,71.

Lyzenga,D.R.,1985, Shallow water bathymetry using combined lidar and passive multispectral scanner data. Int. J. Rem.Sen.,6,115.

Morel.A.,1980, In-water and remote measurements of ocean color. Boundary Layer Met.,18,177.

Parades,J.M., and Spero,R.E., 1983, Water depth mapping from passive remote sensing data under a generalized ratio assumption. Appl. Opt.,22,1134.

Pouwels,H.,1987, Users guide to CAESAR, rapport no: BCRS-87-04.

Preisendorfer, R.V.,1976, Hydrologic Optics, Vol. V (Springfield: U.S. Department of Commerce, NOAA), p.8.

Prieur,L.,1981, Influence of dissolved and suspended matter on inherent properties considered as input parameters in optical ocean modeling. Collection of extended abstracts; Symposium on the radiation transfer in the oceans and remote sensing of ocean properties, IAMAP, Hamburg, p.68.

Prieur,L.,and Sathyendranath,S.,1981, An optical classification of coastal and oceanic water based on the specific spectral absorption curves of phytoplankton pigments, dissolved organic matter, and other particulate materials. Limnol. Oceanogr.,26,671.

Sathyendranath,S.,and Morel,A.,1983, Light emerging from the sea-interpretation and uses in remote sensing. In Remote Sensing Applications in Marine Science and Technology, ed. A.P.Cracknell (Dordrecht: Reidel),p.323.

Smith,R.C., and Baker,K.S.,1981, Optical properties of the clearest natural waters. Appl. Opt.,20,177.

Spitzer,D.,and Dirks,R.W.J.,1985, Contamination of the reflectance of natural waters by solar-induced fluorescence of dissolved organic matter. Appl. Opt.,24,444.

Spitzer,D.,and Dirks,R.W.J.,1986, Chlorophyll fluorescence effects in the red part of reflectance spectra of natural waters. Contin. Shelf. Res.,6,385.

Spitzer,D.,and Dirks,R.W.J.,1987, Bottom influence on the reflectance of the sea. Int. J. Rem. Sen.,8,279.

Tyler,J.E., and Smith,R.C., 1970, Measurements of spectral irradiance under water (New York: Gordon and Breach),p.46.

CONTENTS

Abstract 1

1. Introduction 2

2. Theoretical background 4

3. Input parameters 7

4. Results 10
   4.1. Bottom depth algorithms 11
   4.2. Bottom composition algorithms 15

5. Discussion and conclusion 18

Acknowledgements 20

References 20